HEAD WIDTH INFLUENCES FLOW SENSING BY THE LATERAL LINE CANAL SYSTEM IN FISHES

Yuzo R Yanagitsuru[1,2], Otar Akanyeti[1,3] and James C. Liao[1]

[1]The Whitney Laboratory for Marine Bioscience

[1]Department of Biology

University of Florida

9505 Ocean Shore Blvd, St. Augustine FL USA

[2]Department of Wildlife, Fish, and Conservation Biology

University of California, Davis

[3]Department of Computer Science

Aberystwyth University

Phone: 904-461-4011

Fax: 904-461-4052

E-mail: jliao@whitney.ufl.edu

Key words: lateral line canal system, head morphology, pressure sensing, vortex street

SUMMARY STATEMENT

Fish head width, which varies widely across species, influences how the lateral line canal system can sense both steady and vortical flows.

ABSTRACT

The architecture of the cephalic lateral line canal system, with distinct lines for the supraorbital, infraorbital, and mandibular canals, is highly conserved among fish species. Because these canals lay on a cranial platform, the sensory input they receive is expected to change based on how flow interacts with the head and how the canal pores are spatially distributed. In this study, we explore how head width, a trait that can vary greatly between species and across ontogeny, affects flow sensing. We inserted pressure sensors into physical fish head models of varying widths (narrow, intermediate, and wide) and placed these models in steady and vortical flows. We measured sensory performance in terms of detecting flow parameters (flow speed, vortex shedding frequency, and cylinder diameter), sensitivity, (change in pressure gradient as a function of flow speed) and signal-to-noise ratio (strength of vortex shedding frequency with respect to background). Our results show that in all model heads the amount of hydrodynamic information was maximized at the anterior region regardless of what metric we used to evaluate the sensory performance. In addition, we discovered that all model heads had the highest signal-to-noise ratios (SNR) for vortices at the intermediate flow speeds but that each head width passively optimized the SNR for different sized vortices, which may have implications for refuge and prey seeking. Our results provide insight into the sensory ecology of fishes and has implications for the design of autonomous underwater vehicles.

INTRODUCTION

The lateral line system is used to sense water motion (Dijkgraaf, 1963). This mechanoreceptive organ is critical for performing tasks such as: detecting predators and prey, navigating turbulent flows, and orienting to flows (Coombs et al., 2001; Liao et al., 2003a,b; Montgomery et al., 1997; Pohlmann et al., 2001, 2004; Stewart et al., 2014). The lateral line system is comprised of bundles of flow-sensitive hair cells called neuromasts. There are two types of neuromasts: superficial, which lie directly on top of the skin of fish; and canal neuromasts, which are recessed within open-pored canals running just under the surface of the body and head of fish. Superficial neuromasts are sensitive to flow velocity while canal neuromasts are sensitive to acceleration around the fish and, by extension of Bernoulli's principle, to the pressure differences between adjacent canal pores (Coombs et al., 1988, 1996; Coombs and Janssen, 1990; Haehnel-Taguchi et al., 2014; Kroese and Schellart, 1992).

Fishes exhibit a large anatomical diversity in their lateral line canal; canal diameters, pore spacing, and neuromast shapes vary between species (Carton and Montgomery, 2004; Coombs et al., 1988; Montgomery et al., 1994; van Netten, 2006; Webb, 2013). Canals can also possess features such as membranous pore coverings, branching canal patterns, or localized constrictions within canals, all of which can affect the lateral line's sensitivity to hydrodynamic stimuli (Carton and Montgomery, 2004; Denton and Gray, 1983, 1988; Janssen, 1997, 2004; Montgomery et al., 1994; Webb 1989, 2013). Additionally, fishes exhibit a large diversity of trunk lateral line canal architectures. Many fish have a single, continuous trunk canal on their mid-body. However, depending on the ecology and behavior of a species, the trunk canal architecture may vary. Some fish exhibit a canal line that curves around the pectoral fins, possibly to reduce the hydrodynamic noise generated by the motions of the pectoral fins during swimming (Webb, 1989). Fishes that refuge within tubes or holes may have incomplete canals that run only halfway along their bodies. Others that occupy habitats just below the surface of water or bury themselves in sediment may have ventrally or dorsally located trunk canals, respectively (Webb, 2013).

While relatively little is known about the anatomical diversity of the cephalic lateral line canal across species, the general architecture of the cephalic lateral line canal is highly conserved; it usually consists of three rows: one located above the eye (supraorbital), one below (infraorbital), and one along the lower mandible (mandibular) (Coombs et al., 1988; Webb, 1989, 2013). This conserved architecture becomes particularly interesting when considering the large diversity of fish head morphologies (Alexander and Adams, 2004; Boglino et al., 2013; Bouton et al., 2002; Cabuy et al., 1999; Clabaut et al., 2007; Geerinckx et al., 2007; Kajiura, 2001; Lowry et al., 2007; Tedman, 1980; Wyckmans et al., 2007). When fish swim, flow is induced across the head. How the flow interacts with the head depends greatly on its shape and thus fish heads may receive different sensory inputs depending on morphological variation (Chambers et al, 2014; Herzog et al., 2017). Furthermore, because the fish head is the platform upon which the lateral line lays upon, any differences in head shape alters the spatial position of the lateral line relative to the flow. In this way, the alteration of flows and the difference in spatial positioning of the lateral line induced by head morphology may have important consequences for the ability of fish to sense in their aquatic environment.

To begin exploring how head morphology affects flow detection by the lateral line canal system, we focused initially on one common aspect that is known to vary across species and ontogeny: head width. While possible to directly record from lateral line afferent nerve fibers to evaluate the sensory performance of fishes (Chagnaud et al, 2007; Tricas and Highstein, 1991), it is not trivial to single out the contributions of head width. Instead in this study, we use pressure sensors embedded in 3D printed models with varying head widths to measure pressure gradients. We systematically examine how hydrodynamic information varies as a function of head width and how this may affect the sensing ability of fishes. In particular, we focus on detecting and characterizing two types of flow that fishes regularly encounter in their natural environment: steady and vortical flows.

METHODS

Head Morphometrics.

To help design fish head models, we first collected data from fish species known to have narrow, intermediate, and wide heads. Preserved whole fish specimens were acquired from the Florida Museum of Natural History Ichthyology Collection at University of Florida. All morphometric data was measured using dial calipers. Head length was measured as the distance from the tip of the upper jaw to the posterior margin of the operculum. Head width was measured at the point of maximum width across the head. We normalized head width to head length by calculating aspect ratio (AR = width/length) in order to account for the fact that the head width can span a large range based on the size of the fish. Low and high AR heads would correspond to narrow and wide heads, respectively.

Model heads.

We were interested in understanding the effects of head shape in the anterior-posterior axis. We approximated the curvature of the model heads along this axis as half ellipses using Rhinoceros v5 (Robert McNeel & Associates, Seattle, Washington, USA). We fabricated three models with head widths 2, 6, and 10 cm (Fig. 1A). The length of the models was kept constant at 10 cm. We refer to these models by their AR as narrow (AR=0.2), intermediate (AR=0.6), and wide heads (AR=1.0). The ARs of the models fell within and spanned the naturally occurring range of fish heads (Table 1). Each head was elongated an additional 5.5 cm posterior to the last canal pore to reduce potential effects of having a sharp trailing edge too close to the sensors. This elongation also enabled attachment of the head to a strut located away from the canal pores that positioned the model in the flow tank. In addition, we designed the models relatively tall (i.e. 15 cm) to minimize any 3-dimensional flow effects that may arise on the dorso-ventral axis. To simulate the lateral line canal, heads were designed with pores arranged in a single horizontal line (Fig 1B). There was a single pore at the snout and six pores along the sides. Each pore was 3 mm in diameter and pores were spaced 1 cm apart along the curvature of the head. Thus, sensor position corresponds closely to arc length of head (cm) in our study. Model heads were then 3D printed with acrylonitrile butadiene styrene (ABS) plastic using a Makerbot Replicator 2X (MakerBot^{R} Industries LLC, Brooklyn, New York, USA).

Pressure sensors and experimental setup.

We embedded seven Mikrotip pressure catheters (Millar Instruments, Houston, Texas, USA), one in the snout pore and six on the left side of model heads. The sensors were flush with the surface to minimize sensor-fluid interactions. Pressure sensors were calibrated at one mm below the surface of still water to estimate the value unit conversion to Pascals. Pressure recordings were transmitted via PCU-2000 control units (Millar Instruments, Houston, Texas, USA) and recorded with a sampling rate of 1000 Hz using LabChart (ADInstruments, Dunedin, New Zealand). Experiments were performed in our 175 liter recirculating flow tank. We tested the model heads in steady and vortical flows. Vortical flow (a Kàrmàn vortex street) was generated by placing a stationary cylinder in steady flow (Fig 1C). The working section of the flow tank (25 x 26 x 87 cm; height x width x length) was outfitted with an 80/20 aluminum frame (80/20 Inc.) custom designed to mount heads and cylinders in the working section. To enable repeated positioning of the head in the same region of the flow tank across experiments, heads were secured to the frame from above with a strut. Both heads and cylinders rested against the bottom of the flow tank to prevent self-oscillation.

Pressure measurements.

For steady flow trials, heads were secured to the center of the working area with no cylinder. Pressure was then measured prior to any flow to record mean hydrostatic pressure for all seven sensors simultaneously for 20 seconds. Steady flow was then initiated after which pressure was recorded for 30 seconds. Hydrostatic pressure was also recorded for 30 seconds after flow was stopped to account for potential drift in our sensors. The mean hydrostatic pressure was then subtracted from the steady flow pressure recordings. Because the lateral line canal neuromasts are sensitive to pressure differences between canal pores, we calculated the pressure difference between adjacent sensors for our analyses. Furthermore, because pressure difference is dependent on the distance between pores (van Netten, 2006), we normalized it to the spatial distance between pores for our steady flow measurements. Hereinafter, we refer to this normalized pressure difference as pressure gradient. To assess sensory performance of each head for different sized vortices, we used three different cylinder diameters (1.3, 2.5, 5 cm). The diameter of shed vortices is dictated by cylinder diameter (Liao et al, 2003a), so by using different cylinder sizes we were able to generate vortices that we refer to as: small, medium, and

large for this study. We additionally tested head performance for each vortex size in four flow speeds (26, 52, 79, 105 cm/s) and seven distances from the cylinder (ranging from 3-9 cylinder diameters downstream). Pressure was recorded for 60 seconds for all vortical flow trials. All data analyses were performed using custom written scripts in Matlab 2013b (Mathworks, Natick, Massachusetts, USA), and all values are shown in mean ± standard error of the mean, unless stated otherwise.

Validation of pressure measurements in steady and vortical flows: To validate our empirical measurements, we compared them to those predicted by Bernoulli's Law. For each position along the head, we first calculated the pressure coefficients (C_p) using:

$$C_p = \frac{P}{0.5\rho {U_0}^2} \qquad (1)$$

where P is the measured mean pressure difference between two sensors (Pa), ρ is the density of water at 20°C (998.2 kg m^{-3}), and U_0 is steady flow speed (cm s^{-1}). To calculate the theoretical pressure coefficient ($\hat{C}_p$), we first approximated the local flow speed just outside the boundary layer of a head using the potential flow solution for an elliptical cylinder (Khan et al, 2005):

$$U(s) = \frac{U_0(1+\epsilon)\sin\theta}{\sqrt{1-e^2\cos^2\theta}} \qquad (2)$$

where $U(s)$ is local flow speed (cm s^{-1}) at s arc length of head (cm), ϵ is AR of head, θ is the angle measured from the snout, and e is eccentricity = $\sqrt{1-\epsilon^2}$. We then input $U(s)$ to Equation 3 to calculate $\hat{C}_p$.

$$\hat{C}_p = 1 - \left(\frac{U(s)}{U_0}\right)^2 \qquad (3)$$

Pressure measurements in vortical flows fluctuated over time due to the presence of vortices (Fig 1D). To measure the strength of these fluctuations, we calculated the standard deviation of pressure difference over time and normalized it to sensor spacing. We then converted pressure fluctuations to C_p using equation 1. We then evaluated the fit of the

Bernoulli-derived $\hat{C}_p$ by calculating the mean absolute error between measured C_p and predicted $\hat{C}_p$.

Sensitivity to changes in flow speed: To examine how well a model head could theoretically detect changes in flow speed we define sensitivity as the change in pressure gradient induced by a unit change in flow speed. Thus, the larger the change in pressure gradient, the higher the sensitivity. During steady and vortical flows, we observed that pressure gradient at each point along the head increased linearly with flow speed. Therefore, we calculated sensitivity from the slope of the linear fit between pressure gradient and flow (Fig. 2C). We also evaluated the goodness of the linear fit using coefficient of determination (R^2 value). In addition, to identify how sensitivity varies along the head, we first selected the data points with R^2>0.8, and then fit an exponential curve ($y=ae^{bx}+c$). The parameters of the exponential curve (a, b and c) were estimated using least square methods.

Signal-to-noise ratio (SNR): We evaluated the ability of model heads to detect the periodicity of the vortical flows (i.e. vortex shedding frequency). We first obtained the frequency spectrum of pressure measurements using fast-Fourier transform and identified the frequency with maximum amplitude (i.e. dominant frequency). After confirming that the dominant frequency matched the expected vortex shedding frequency (i.e. desired signal), we calculated the SNR by dividing the amplitude of the desired signal by the noise amplitude (i.e. amplitudes of other frequencies). We estimated the noise amplitude as described in a previous study. (Miersch et al., 2011). For each model head at a given trial, we compared the SNR values along the head and chose the maximum one. To determine the effects of head width, vortex size, flow speed, and cylinder position on maximum SNR, we used a four-way ANOVA at an α level of 0.05 (and subsequent Tukey's multiple comparison post hoc test).

Estimating flow parameters using pressure measurements

We used pressure measurements to estimate the flow speed, vortex shedding frequency and cylinder diameter. To estimate the flow speed, we input actual pressure measurements and predicted $\hat{C}_p$ into Equation 4,

$$U_0 = \sqrt{\frac{P}{0.5\rho\hat{C}_p}} \qquad (4)$$

We calculated the theoretical vortex shedding frequencies (f_{exp}) for each cylinder diameter and flow speed combination using Equation 5,

$$f_{exp} = \frac{StU_0}{D} \qquad (5)$$

where St is the Strouhal number (0.2) appropriate for the Reynolds numbers of our experiments (3,300-53,000) (Blevins, 1990), and D is cylinder diameter (cm). Finally, using the flow speed calculated from Equation 4 and the mean vortex shedding frequency, we calculated the cylinder diameter using Equation 5. We then compared the measured and predicted flow parameters by calculating the mean absolute error.

RESULTS

Pressure measurements in steady flows

Pressure gradient increased with flow speed and the maximum pressure gradients were concentrated at the front of the model heads (Fig 2A). The maximum pressure gradients experienced by the narrow head was higher than those experienced by the wider heads. However, the region of maximum pressure gradient was substantially smaller in the narrow head than in the wider heads. For example, in the narrow head pressure gradient dropped from maxima to minima at P2-P3 (Fig Ai), whereas in the intermediate and wide heads the pressure gradient dropped to minima at P3-P4 and P6-P7, respectively (Fig Aii-iii). Our results show that C_p profiles along the narrow and intermediate head did not change with flow speed, and they closely matched with theoretical predictions (Fig. 2Bi-ii). The mean absolute error between measured and predicted C_p were 0.04 and 0.06 for the narrow and intermediate heads, respectively. In contrast, we found that the C_p profile along the wide head changed with flow speed, and there was a larger difference between measured and predicted C_p with mean absolute error 0.12 (Fig. 2Biii). This may have been due to the fluid-structure interactions caused by the more constricted environment inherent to the wide head in a flow tank of finite width relative to narrow and intermediate heads. We found that the sensitivity profiles of the heads closely reflected their pressure gradient and C_p profiles (Fig 2C). Sensitivity along all heads decreased across sensor

position exponentially ($y=ae^{bx}+c$) with the following parameters: narrow ($a=1626*10^6$, b=-12.69, c=-0.15), intermediate (a=40.05, b=-1.13, c=0.18), and wide (a=951.8, b=-0.0005, c=-947.8). The maximum sensitivity experienced by the narrow head was higher but limited to a smaller anterior region than those experienced by the wider heads. The sensitivity of the narrow, intermediate, and wide heads dropped below 20% of the maximum sensitivity measured at 9.6, 25.1, and 49.0% of head arc length, respectively. Pressure measurements in steady flows did not experience any fluctuation, indicating that if any vortices were shed from the trailing edge of the models, they still had no influence on the pressure gradient along the head (Bearman, 1984).

Pressure measurements in vortical flows

Similar to the pressure gradient profiles in steady flows, the maximum pressure fluctuation points were concentrated at the front of the model heads, and the maximum pressure fluctuation experienced by the narrow head was higher than those experienced by the wider heads. (Fig. 3A). This was true regardless of the flow speed or cylinder size (i.e. vortex size) (Fig. 3A-B). In the narrow and intermediate heads, pressure fluctuation at P1-P2 increased with vortex size but remained constant in the wide head (Fig 3B). At 26 cm s^{-1}, C_p profiles along the narrow and intermediate heads were consistently higher than C_p of other flow speeds. We found that the sensitivity of the model heads was significantly lower in vortical flows than in steady flows (i.e. up to 1000 times less at the front of the head). Similar to steady flows, the sensitivity profiles of the heads closely reflected their pressure and C_p profiles (Fig 3D). Sensitivity along all heads decreased across sensor position exponentially with the following parameters: narrow (a=23.90, b=-1.517, c=0.4672), intermediate (a=9.902, b=-1.175, c=0.5474), and wide (a=3.269, b=-1.198, c=1.089). The maximum sensitivity experienced by the narrow head was higher but limited to a smaller anterior region than those experienced by the wider heads. The sensitivity of the narrow and intermediate heads dropped below 20% of the maximum sensitivity at 36.1 and 49.0% of head arc length, respectively. The sensitivity of the wide head never dropped below 20% of the maximum sensitivity measured for vortical flows.

Estimating vortex shedding frequency, flow speed and cylinder diameter

To calculate the flow parameters, we averaged the pressure gradient and pressure fluctuation from the regions with sensitivities higher than 20% of the maximum sensitivity for steady and vortical flows, respectively (see Fig 2C and 3D). In steady flows, this corresponded to P1-P2 for the narrow head, P1-P2 and P2-P3 for the intermediate and wide heads (Fig. 2C). In vortical flows, this corresponded to P1-P2 for the narrow head, P1-P2, P2-P3, and P3-P4 for the intermediate head and P1-P2, P2-P3, P3-P4, P4-P5, P5-P6, and P6-P7 for the wide head (Fig. 3C). Our results show that all heads could accurately identify the vortex shedding frequency with a prediction error less than 10%, regardless of the flow speed or cylinder size (Fig. 4A). The heads were also successful in estimating the flow speed in both flow regimes (Fig. 4B-C). Their prediction error for steady flow was less than 20%. The prediction error for vortical flows was less than 15% except at the lowest flow speed (26 cm s^{-1}), which had prediction errors between 10 and 30%. After estimating the vortex shedding frequency and flow speed, we recovered the cylinder diameter using Equation 5 with a prediction error less than 15% except for the lowest flow speed (Fig. 4D). At the lowest flow speed, heads yielded prediction errors between 20 and 65% likely due to the high error associated with estimating that particular flow speed.

Detecting incoming vortices

In all model heads, SNR was maximum at the front part of the head (i.e. P1-P2) and decreased gradually across sensor position (Fig. 5A). This trend was independent from the flow speed and vortex sizes tested. On average, SNRs were higher for medium and large vortices than for small vortices. We found that SNRs were highest at the intermediate flow speeds (i.e. 52 cm s^{-1} and 79 cm s^{-1}; Fig. 5B). SNR varied greatly with distance but did not follow any predictable pattern (Fig. 5C). When we look at the overall performance of each model head, we find that sensitivity for a given vortex size varied with head width (Fig. 6). For small vortices, the narrow head had the highest SNR (15.10±0.24 dB) followed by the intermediate head (13.8±0.24 dB) and then wide head (11.1±0.23 dB). For medium vortices, the narrow and intermediate heads had the highest SNRs (20.7±0.30 dB and 20.4±0.21 dB, respectively), whereas the wide head had the lowest SNR (14.68±0.24 dB). For large vortices, the intermediate head had the highest SNR (21.57±0.19 dB), followed by the narrow (19.68±0.41 dB) and then wide head (17.78±0.34 dB).

DISCUSSION

Hydrodynamic signal is greatest at the anterior region

In this study, sensitivity, pressure fluctuation, and SNR are greatest at the snout regardless of head width or flow condition. Pressure gradient in steady flows was also greatest at the snout for narrow and intermediate heads and just behind the snout for wide heads. Thus, when a fish is oriented upstream in both steady and vortical flows, the most flow information for the lateral line canal is available at the anterior head region (directly at the snout or just behind) in steady flows. Previous experimental and computation studies in steady flows reveal similar pressure distributions (Akanyeti et al, 2013; Ristroph et al, 2015; Herzog et al, 2017). Moreover, flow imaging and modeling studies show that gliding in real fish, of which our study most closely approximates, experience the largest pressure gradient at the anterior region of the head during obstacle avoidance and wall following behaviors (Windsor et al, 2010a,b). During steady swimming, fish continuously heave and yaw their head during steady swimming, which also has the potential to alter the pressure profile along the head (Lighthill, 1993; Akanyeti et al, 2016). It is remarkable, then, that across the different conditions of flow and swimming behaviors, the distribution of pressure stimuli along the head of fish remains similar in that the snout remains the most sensitive to external stimuli (Dubois et al, 1974; Akanyeti et al, 2016). These results suggest that the anterior region of the head has access to a rich area of hydrodynamic information for the lateral line canal. It would be of great interest in future studies to examine the anatomy of anterior canals in more detail to see whether any anatomical specializations were selected for in regions where hydrodynamic information is greatest (Coombs et al, 1988; Webb, 1989, 2013; Ristroph et al, 2015; Windsor et al, 2010a).

Ecological applications of sensing vortices

Fish hold station behind objects to take refuge from fast flows (Johansen et al., 2008; Liao et al 2003a, Krause et al., 1998; Sutterlin and Waddy, 1975). To do so, fish can adjust their swimming gait to slalom between vortices shed by a stationary object in flow (i.e. Kármán gait), allowing them to significantly reduce the cost of locomotion (Liao et al., 2003a, b; Taguchi and Liao, 2011). Trout are able to Kármán gait across several different flow speeds and cylinder sizes, but prefer certain conditions (Akanyeti and Liao, 2013; Liao et al., 2003a; Liao, 2006). This preference across flow speeds may be mediated by the lateral line, since in the absence of vision, trout will still Kármán gait (Liao, 2006).

We found that SNR for vortices was highest at intermediate flow speeds, regardless of head width. These speeds correlate with the flow speeds at which rainbow trout are most likely to Kármán gait (Akanyeti and Liao, 2013). Intermediate flow speeds likely have higher SNRs due to the shedding of stronger, more coherent vortices with less noise. This is in comparison to lower and higher flow speeds, which have weaker vortices and more turbulence, respectively (Blevins, 1990). The correlation between the likelihood to Kármán gait and a high SNR suggests that active sensing could play a role in Kármán gaiting (Liao 2003a,b, 2006). Furthermore, fish will only Kármán gait behind an appropriately sized cylinder (Liao et al 2003b; Akanyeti and Liao 2013). We found that the width of the head optimizes the detection of vortices by the canal system, whereby wide heads are more sensitive to detecting larger vortices than smaller vortices, and narrow heads are more sensitive to detecting smaller vortices than larger vortices. Within species, there is evidence that the ratio of head width to body length does not vary much across development (Ceas and Page, 1996; Randall and Page, 2012; Wright and Page, 2008). Thus, as an individual fish grows, it may continue to passively optimize the detection of vortices from which it can best refuge. Across species, we suggest that fish with wider heads will detect vortical flows with the larger vortices and vice versa. This may lead to preferences in refuging locations and thus hold implications for differential habitat utilization between species of different head widths. The inability to record neural activity from the lateral line cephalic canal system makes it challenging to understand what flow information is actually detected by the head of a fish during swimming. However, this study provides a fundamental advance in our understanding by simply describing what information is *available* to the canal system along the fish head. While we know that fishes can detect and exploit vortices in nature, this study is the first to show how the amount of hydrodynamic information available to fish is shaped by the head in different flow conditions.

Animals that undulate in water generate vortex wakes that the lateral line can sense (Gardiner and Atema, 2007, Hanke and Bleckman, 2004; Pohlmann et al., 2001, 2004). These thrust wakes (as opposed to drag wakes) contain information such as tailbeat frequency and amplitude of the swimming prey, which can be used to estimate the animal's swimming speed and size (Blickhan et al., 1992; Hanke et al., 2000, 2004; Müller et al., 1997). Our study suggests that in addition to facilitating the ability to seek optimal flow refuges, the natural tuning to specific vortex sizes could allow fish to passively size-select optimal prey even in low-light

environments, which could maximize energy gains (Kislalioglu and Gibson, 1976; Prejs et al., 1990). Furthermore, we provide evidence that the lateral line canal can be used to identify cylinder sizes and flow speeds, which suggest that it is possible in theory for fish to actively differentiate between prey size and identify swimming speeds. However, verification of this ability awaits experiments on live fish.

While neural mechanisms such as the particular response properties of afferent neurons may enhance the ability to detect vortices, a hydrodynamic mechanism that could contribute to our observation that head width self-selects for vortex size detection is vortex rebound. Vortex rebound occurs when a vortex contacts, and then rebounds off of, a broad surface such as the head (Orlandi, 1990). In the case of Kármán vortex streets where vortices are continually shed into the wake, a vortex could rebound from the head and interfere with the next oncoming vortex. This would diminish the strength and periodicity of the vortex street in the region of the head. Because the wider the head, the more it approximates a straight wall to an inbound vortex (particularly for smaller vortices), we believe that vortex rebound may be responsible for reducing SNR when intermediate and wide heads interact with small vortices generated by a small cylinder. We believe that fluid-structure interactions dictate the patterns in SNR we observed. However, our experimental design could not distinguish whether the differences in SNR were due to fluid interactions, or small differences in the spatial distribution of sensors, across different head widths. Further studies into the mechanism underlying vortex size discrimination would benefit from computational models, given that the large size of pressure sensors in experimental studies limits the resolution of spatial sampling of canal pores.

Flows in nature are often much more complex than vortex streets, arising from the fluid-structure interactions of multiple objects. While our analyses focus on characterizing the hydrodynamic information available in unsteady flows induced by a single cylinder, a fertile area for future experiments would be to evaluate how more complex environments may be perceived and how they can be assessed by the pressure-sensing lateral line canal system. For example, two cylinders arranged in tandem can significantly alter the strength and shedding frequency of vortices, which changes when and how fish Kármán gait (Stewart et al., 2016). In this context, it would be interesting to evaluate how pressure sensing plays a role in how fish decide to position themselves around aggregate structures in flow.

Implications for Roboticists

Flow sensors provide crucial information for autonomous underwater vehicles (AUVs) seeking to navigate complex and novel environments (Devries et al., 2015; Salumäe and Kruusmaa, 2013; Tan, 2011). Both physical and mathematical models have shown that a linear array of pressure sensors can be used to accurately determine environmental flow speeds, characterize vortex wakes, and localize objects (Chambers et al., 2014; Ćurčić-Blake and van Netten, 2006; Franosch et al., 2009; Klein and Bleckman, 2011; McConney et al., 2009; Pandya et al., 2006; Ren and Mohseni, 2012; Venturelli et al., 2012; Yang et al. 2006, 2010). While all model heads could accurately estimate several steady flow parameters in our study, they used different subsets of sensors to do this. Narrow heads were only able to accurately determine flow speeds by using the pressure measurements at the front part of the head. The intermediate and wide heads, on the other hand, could most accurately determine flow speeds by averaging measurements across a larger region of the head. This suggests that narrow heads need fewer sensors to detect flow speed compared to wider heads. Coupled with the relatively larger sensitivity to change in flow speed towards the snout, a narrow sensor platform appears optimal for velocity detection on an AUV. Furthermore, head width had minimal effect on how accurately vortex shedding frequency, flow speed, and cylinder size within a Kármán vortex street could be determined. Taken together, we recommend a narrow sensor platform for use on AUVs to minimize the number of sensors required to detect and characterize both steady and vortical flows.

Our two-dimensional study on head width focused on only one aspect of head morphology. AUV sensor placement must be designed to represent a three-dimensional structure that possesses substantial dorso-ventral curvature. Another rich area of investigation would be the influence of surface topography on flow sensing. Microscopic depressions observed on heads of the ide (*Leuciscus idus*) called epidermal pits have been suggested to increase SNRs by 10-30 dB when detecting predators or prey (Herzog et al., 2017). This becomes particularly interesting when considering the large diversity of fish scale morphologies that exist (Agassiz, 1833; Roberts, 1993). Future studies on the three-dimensional head morphologies and surface topographies promise to provide insight on how to enhance the sensitivity and efficiency of AUV sensor platforms.

Acknowledgements

We would like to thank William Stewart, Lawrence Page, Lawrence Ukeiley, and David Blackburn for helpful discussions throughout the project. Comments from two anonymous reviewers improved the manuscript substantially.

Competing Interests

The authors declare no competing or financial interests.

Author Contributions

Y.R.Y., O.A. and J.C.L. designed the study. Y.R.Y. and O.A. conducted the pressure experiments. Y.R.Y. and O.A. analyzed the data. Y.R.Y., O.A. and J.C.L. interpreted the data. Y.R.Y. and J.C.L. wrote the manuscript.

Funding

This work was supported by the National Institutes of Health [1RO1DC010809-01] and National Science Foundation [IOS-1257150] to J.C.L.

References

Agassiz, L. (1833). Recherches sur les poissons fossiles: Tome 2 (Vol. 2). Petitpierre.

Akanyeti, O. and Liao, J.C. (2013). The effect of flow speed and body size on Kármán gait kinematics in rainbow trout. J. Exp. Biol., **216**, 3442-3449.

Akanyeti, O., Chambers, L.D., Ježov, J., Brown, J., Venturelli, R., Kruusmaa, M., Megill, W.M. and Fiorini, P. (2013). Self-motion effects on hydrodynamic pressure sensing: part I. Forward–backward motion. Bioinspir. Biomim., **8**, 026001.

Akanyeti, O., Thornycroft, P. J. M., Lauder, G. V., Yanagitsuru, Y. R., Peterson, A. N., & Liao, J. C. (2016). Fish optimize sensing and respiration during undulatory swimming. Nat commun, **7**.

Alexander, G.D. and Adams, C.E. (2004). Exposure to a common environment erodes inherited between- population trophic morphology differences in Arctic charr. J. Fish Biol., **64**, 253-257.

Bearman, P.W. (1984). Vortex shedding from oscillating bluff bodies. Annu. Rev. Fluid Mech., **16**(1), 195-222.

Blevins, R. D. (1990). Flow-induced vibration.

Blickhan, R., Krick, C., Zehren, D., Nachtigall, W. and Breithaupt, T. (1992). Generation of a vortex chain in the wake of a Suhundulatory swimmer. Naturwissenschaften, **79**, 220-221.

Boglino, A., Wishkerman, A., Darias, M.J., Andree, K.B., De la Iglesia, P., Estévez, A. and Gisbert, E. (2013). High dietary arachidonic acid levels affect the process of eye migration and head shape in pseudoalbino Senegalese sole Solea senegalensis early juveniles. J. Fish Biol., **83**, 1302-1320.

Bouton, N., Visser, J.D. and Barel, C.D. (2002). Correlating head shape with ecological variables in rock- dwelling haplochromines (Teleostei: Cichlidae) from Lake Victoria. Biol. J. Linnean Soc., **76**, 39-48.

Cabuy, E., Adriaens, D., Verraes, W. and Teugels, G.G. (1999). Comparative study on the cranial morphology of Gymnallabes typus (Siluriformes: Clariidae) and their less anguilliform relatives, Clariallabes melas and Clarias gariepinus. J. Morphol., **240**, 169-194.

Carton, A.G. and Montgomery, J.C. (2004). A comparison of lateral line morphology of blue cod and torrentfish: two sandperches of the family Pinguipedidae. Env. Biol. Fish, **70**, 123-131.

Ceas, P.A. and Page, L.M. (1996). Chaetostoma yurubiense (Teleostei: Siluriformes), a new species of loricariid catfish from the Aroa, Urama, and Yaracuy river systems in Venezuela. Copeia 671-677.

Chagnaud, B.P., Bleckmann, H. and Hofmann, M.H. (2007). Kármán vortex street detection by the lateral line. J. Comp. Physiol. A, **193**, 753-763.

Chambers, L.D., Akanyeti, O., Venturelli, R., Ježov, J., Brown, J., Kruusmaa, M., Fiorini, P. and Megill, W.M. (2014). A fish perspective: detecting flow features while moving using an artificial lateral line in steady and unsteady flow. J. R. Soc. Interface, **11**, 20140467.

Ciccotto, P. J., & Page, L. M. (2016). From 12 to one species: variation in Lobocheilos rhabdoura (Fowler, 1934) (Cyprinidae: Labeonini). Copeia, **104**, 879-889.

Clabaut, C., Bunje, P.M., Salzburger, W. and Meyer, A. (2007). Geometric morphometric analyses provide evidence for the adaptive character of the Tanganyikan cichlid fish radiations. Evolution, **61**, 560-578.

Coombs, S., Janssen, J. and Webb, J.F. (1988). Diversity of lateral line systems: evolutionary and functional considerations. In Sensory biology of aquatic animals, pp. 553-593, Springer New York.

Coombs, S. and Janssen, J. (1990). Behavioral and neurophysiological assessment of lateral line sensitivity in the mottled sculpin, Cottus bairdi. J. Comp. Physiol. A, **167**, 557-567.

Coombs, S., Hastings, M. and Finneran, J. (1996). Modeling and measuring lateral line excitation patterns to changing dipole source locations. J. Comp. Physiol. A: Neuroethology, Sensory, Neural, and Behavioral Physiology, **178**, 359-371.

Coombs, S., Braun, C.B. and Donovan, B. (2001). The orienting response of Lake Michigan mottled sculpin is mediated by canal neuromasts. J. Exp. Biol., **204**, 337-348.

Ćurčić-Blake, B. and van Netten, S.M. (2006). Source location encoding in the fish lateral line canal. J. Exp. Biol., **209**, 1548-1559.

Denton, E.J. and Gray, J. (1983). Mechanical factors in the excitation of clupeid lateral lines. Proc. R. Soc. Lond. B Biol. Sci., **218**, 1-26.

Denton, E. J., & Gray, J. A. (1988). Mechanical factors in the excitation of the lateral lines of fishes. In *Sensory biology of aquatic animals* (pp. 595-617). Springer, New York, NY.

DeVries, L., Lagor, F.D., Lei, H., Tan, X. and Paley, D.A. (2015). Distributed flow estimation and closed-loop control of an underwater vehicle with a multi-modal artificial lateral line. Bioinspir. Biomim, **10**, 025002.

Dijkgraaf, S. (1963). The functioning and significance of the lateral- line organs. Biol. Rev. Camb. Philos. Soc. **38**, 51-105.

Dubois, A. B., Cavagna, G. A., & Fox, R. S. (1974). Pressure distribution on the body surface of swimming fish. J. Exp. Biol., **60**, 581-591.

Franosch, J. M. P., Hagedorn, H. J., Goulet, J., Engelmann, J., & van Hemmen, J. L. (2009). Wake tracking and the detection of vortex rings by the canal lateral line of fish. Phys. Rev. Lett., **103**, 078102.

Gardiner, J.M. and Atema, J. (2007). Sharks need the lateral line to locate odor sources: rheotaxis and eddy chemotaxis. J. Exp. Biol., **210**, 1925-1934.

Geerinckx, T., Brunain, M., Herrel, A., Aerts, P. and Adriaens, D. (2007). A head with a suckermouth: a functional-morphological study of the head of the suckermouth armoured catfish Ancistrus cf. triradiatus (Loricariidae, Siluriformes). Belg. J. Zool., **137**, 47.

Haehnel-Taguchi, M., Akanyeti, O. and Liao, J.C. (2014). Afferent and motoneuron activity in response to single neuromast stimulation in the posterior lateral line of larval zebrafish. *J. Neurophysiol*, **112**, 1329-1339.

Hanke, W., Brucker, C. and Bleckmann, H. (2000). The ageing of the low-frequency water disturbances caused by swimming goldfish and its possible relevance to prey detection. J. Exp. Biol., **203**, 1193-1200.

Hanke, W. and Bleckmann, H. (2004). The hydrodynamic trails of Lepomis gibbosus (Centrarchidae), Colomesus psittacus (Tetraodontidae) and Thysochromis ansorgii (Cichlidae) investigated with scanning particle image velocimetry. J. Exp. Biol., **207**, 1585-1596.

Herzog, H., Klein, B. and Ziegler, A. (2017). Form and function of the teleost lateral line revealed using three-dimensional imaging and computational fluid dynamics. J. R. Soc. Interface, **14**, 20160898.

Janssen, J. (1997). Comparison of response distance to prey via the lateral line in the ruffe and yellow perch. J. Fish Biol., **51**, 921-930.

Janssen, J. (2004). Lateral line sensory ecology. In The Senses of Fish, pp. 231-264, Springer Netherlands.

Johansen, J.L., Bellwood, D.R. and Fulton, C.J. (2008). Coral reef fishes exploit flow refuges in high-flow habitats. Marine Ecology Progress Series, **360**, 219-226.

Kajiura, S.M. (2001). Head morphology and electrosensory pore distribution of carcharhinid and sphyrnid sharks. Env. Biol. Fish., **61**, 125-133.

Khan, W.A., Culham, R.J. and Yovanovich, M.M. (2005). Fluid flow around and heat transfer from elliptical cylinders: analytical approach. J. Thermophys. Heat Transfer **19**. 178-185.

Kislalioglu, M. and Gibson, R.N. (1976). Prey 'handling time'and its importance in food selection by the 15-spined stickleback, Spinachia spinachia (L.). J. Exp. Mar. Biol. Ecol., **25**, 151-158.

Klein, A. and Bleckmann, H. (2011). Determination of object position, vortex shedding frequency and flow velocity using artificial lateral line canals. Beilstein J. Nanotechnol., **2**, 276-283.

Krause, J., Loader, S.P., McDermott, J. and Ruxton, G.D. (1998). Refuge use by fish as a function of body length–related metabolic expenditure and predation risks. Proceedings of the Royal Society of London B: Biological Sciences, **265**, 2373-2379.

Kroese, A.B. and Schellart, N.A. (1992). Velocity-and acceleration-sensitive units in the trunk lateral line of the trout. J. Neurophysiol., **68**, 2212-2221.

Liao, J.C., Beal, D.N., Lauder, G.V. and Triantafyllou, M.S. (2003a). Fish exploiting vortices decrease muscle activity. Science **302**, 1566-1569.

Liao, J.C., Beal, D.N., Lauder, G.V. and Triantafyllou, M.S. (2003b). The Karman gait: novel body kinematics of rainbow trout swimming in a vortex street. J. Exp. Biol. **206**, 1059-1073.

Liao, J.C. (2006). The role of the lateral line and vision on body kinematics and hydrodynamic preference of rainbow trout in turbulent flow. J. Exp. Biol. **209**, 4077-4090.

Lighthill, J. (1993). Estimates of pressure differences across the head of a swimming clupeid fish. Phil. Trans. R. Soc. Lond. B, **341**(1296), 129-140.

Lowry, D., Motta, P.J. and Hueter, R.E. (2007). The ontogeny of feeding behavior and cranial morphology in the leopard shark Triakis semifasciata (Girard 1854): a longitudinal perspective. J. Exp. Mar. Biol. Ecol., **341**, 153-167.

McConney, M.E., Chen, N., Lu, D., Hu, H.A., Coombs, S., Liu, C. and Tsukruk, V.V. (2009). Biologically inspired design of hydrogel-capped hair sensors for enhanced underwater flow detection. Soft Matter, **5**, 292-295.

Miersch, L., Hanke, W., Wieskotten, S., Hanke, F. D., Oeffner, J., Leder, A., Brede, M., Witte, M., & Dehnhardt, G. (2011). Flow sensing by pinniped whiskers. Phil. Trans. R. Soc. B, **366**(1581), 3077-3084.

Montgomery, J., Coombs, S. and Janssen, J. (1994). Form and function relationships in lateral line systems: comparative data from six species of Antarctic notothenioid fish. Brain Behav. Evol., **44**, 299-306.

Montgomery, J.C., Baker, C.F. and Carton, A.G. (1997). The lateral line can mediate rheotaxis in fish. Nature **389**, 960-963.

Müller, U.K., Van Den Heuvel, B.L.E., Stamhuis, E.J. and Videler, J.J. (1997). Fish foot prints: morphology and energetics of the wake behind a continuously swimming mullet (Chelon labrosus Risso). J. Exp. Biol. **200**, 2893-2906.

Orlandi, P. (1990). Vortex dipole rebound from a wall. Phys. Fluids A **2**, 1429-1436.

Pandya, S., Yang, Y., Jones, D.L., Engel, J. and Liu, C. (2006). Multisensor processing algorithms for underwater dipole localization and tracking using MEMS artificial lateral-line sensors. EURASIP J. App. Signal Process., **2006**, 199-199.

Prejs, A., Lewandowski, K. and Stańczykowska-Piotrowska, A. (1990). Size-selective predation by roach (Rutilus rutilus) on zebra mussel (Dreissena polymorpha): field stuides. Oecologia, **83**, 378-384.

Pohlmann, K., Grasso, F.W. and Breithaupt, T. (2001). Tracking wakes: the nocturnal predatory strategy of piscivorous catfish. Proc. Natl. Acad. Sci. **98**, 7371-7374.

Pohlmann, K., Atema, J. and Breithaupt, T. (2004). The importance of the lateral line in nocturnal predation of piscivorous catfish. J. Exp. Biol. **207**, 2971-2978.

Randall, Z.S. and Page, L.M. (2012). Resurrection of the genus Homalopteroides (Teleostei: Balitoridae) with a redescription of H. modestus (Vinciguerra 1890). Zootaxa **3586**, 329-346.

Ren, Z. and Mohseni, K. (2012). A model of the lateral line of fish for vortex sensing. Bioinspir. Biomim., **7**, 036016.

Ristroph, L., Liao, J. C., & Zhang, J. (2015). Lateral line layout correlates with the differential hydrodynamic pressure on swimming fish. Phys. Rev. Lett., **114**, 018102.

Roberts, C. D. (1993). Comparative morphology of spined scales and their phylogenetic significance in the Teleostei. Bull. Mar. Sci., **52**, 60-113.

Salumäe, T. and Kruusmaa, M. (2013), May. Flow-relative control of an underwater robot. In Proc. R. Soc. A **2153**, 20120671. The Royal Society.

Stewart, W.J., Nair, A., Jiang, H. and McHenry, M.J. (2014). Prey fish escape by sensing the bow wave of a predator. J. Exp. Biol. **217**, 4328-4336.

Stewart, W. J., Tian, F. B., Akanyeti, O., Walker, C. J., & Liao, J. C. (2016). Refuging rainbow trout selectively exploit flows behind tandem cylinders. J. Exp. Biol., **219**, 2182-2191.

Sutterlin, A.M. and Waddy, S. (1975). Possible role of the posterior lateral line in obstacle entrainment by brook trout (Salvelinus fontinalis). J. Fish. Res. Bd. Can., **32**, 2441-2446.

Taguchi, M. and Liao, J.C. (2011). Rainbow trout consume less oxygen in turbulence: the energetics of swimming behaviors at different speeds. J. Exp. Biol. **214**, 1428-1436.

Tan, X. (2011). Autonomous robotic fish as mobile sensor platforms: Challenges and potential solutions. *Marine Technology Society Journal*, **45**, 31-40.

Tedman, R.A. (1980). Comparative study of the cranial morphology of the labrids Choeroden venustus and Labroides dimidiatus and the scarid Scarus fasciatus (Pisces: Perciformes) II. Cranial myology and feeding mechanisms. Marine and Freshwater Research, **31**, 351-372.

Tricas, T.C. and Highstein, S.M. (1991). Action of the octavolateralis efferent system upon the lateral line of free-swimming toadfish, Opsanus tau. J. Comp. Physiol. A, **169**, 25-37.

van Netten, S.M. (2006). Hydrodynamic detection by cupulae in a lateral line canal: functional relations between physics and physiology. Biol cybern, **94**, 67-85.

Venturelli, R., Akanyeti, O., Visentin, F., Ježov, J., Chambers, L. D., Toming, G., Brown, J., Kruusmaa, M., Megill, W.M., & Fiorini, P. (2012). Hydrodynamic pressure sensing with an artificial lateral line in steady and unsteady flows. Bioinspir. Biomim., *7*(3), 036004.

Webb, J.F. (1989). Gross Morphology and Evolution of the Mechanoreceptive Lateral-Line System in Teleost Fishes (Part 1 of 2). Brain Behav Evol. **33**, 34-43.

Webb, J.F. (2013). Morphological diversity, development, and evolution of the mechanosensory lateral line system. In The lateral line system, pp. 17-72, Springer New York.

Windsor, S.P., Norris, S.E., Cameron, S.M., Mallinson, G.D. and Montgomery, J.C. (2010a). The flow fields involved in hydrodynamic imaging by blind Mexican cave fish (Astyanax fasciatus). Part I: open water and heading towards a wall. J. Exp. Biol., **213**, 3819-3831.

Windsor, S.P., Norris, S.E., Cameron, S.M., Mallinson, G.D. and Montgomery, J.C. (2010b). The flow fields involved in hydrodynamic imaging by blind Mexican cave fish (Astyanax fasciatus). Part II: gliding parallel to a wall. J. Exp. Biol., **213**, 3832-3842.

Wright, J.J. and Page, L.M. (2008). A new species of Synodontis (Siluriformes: Mochokidae) from tributaries of the Kasai River in Northern Angola. Copeia **2008**, 294-300.

Wyckmans, M., Van Wassenbergh, S., Adriaens, D., Van Damme, R. and Herrel, A. (2007). Size- related changes in cranial morphology affect diet in the catfish Clariallabes longicauda. Biol. J. Linnean Soc., **92**, 323-334.

Yang, Y., Chen, J., Engel, J., Pandya, S., Chen, N., Tucker, C., Coombs, S., Jones, D.L. and Liu, C. (2006). Distant touch hydrodynamic imaging with an artificial lateral line. Proc. Natl. Aca. Sci., **103**, 18891-18895.

Yang, Y., Nguyen, N., Chen, N., Lockwood, M., Tucker, C., Hu, H., Bleckmann, H., Liu, C. and Jones, D.L. (2010). Artificial lateral line with biomimetic neuromasts to emulate fish sensing. Bioinspir. Biomim., **5**, 016001.

Table 1. Minimum and maximum aspect ratios (width/length) for fish species from different families collected at the Florida Natural History Museum Ichthyology Collection or obtained from literature.

Family	Species	Aspect Ratios	Sources
Belonidae	*Ablennes hians* (n=3)	0.09-0.14	UF 98370, 98367, 79355
Lepisosteidae	*Lepisosteus osseus* (n=4)	0.14-0.16	UF 94021, 79515, 16019
Carangidae	*Selene vomer* (n=3)	0.21-0.26	UF 184035, 13916, 178
Acipenseridae	*Acipenser fulvescens* (n=3)	0.32-0.43	UF 174970, 2375, 7324
Salmonidae	*Oncorhynchus mykiss* (n=3)	0.45-0.52	UF 99412, 97536, 89979
Chimaeridae	*Hydrolagus alberti* (n=3)	0.45-0.53	UF 213861, 232909, 17314
Cyprinidae	*Lobocheilos rhabdoura* (n=177)	0.48-0.79	Ciccotto and Page 2016
Serranidae	*Centropristis striates* (n=3)	0.51-0.62	UF 139179, 151775, 68498
Triakidae	*Mustelus canis* (n=3)	0.57-0.67	UF 101329, 101320, 16549
Balitoridae	*Homalopteroides modestus* (n=68)	0.57-0.77	Randall and Page 2012
Loricariidae	*Chaetostoma yurubiense* (n=13)	0.72-0.89	Ceas and Page 1996
Sisoridae	*Bagarius bagarius* (n=13)	0.73-0.87	UF 237527, 176582
Loricariidae	*Opsanus tau* (n=3)	0.79-0.89	Ceas and Page 1996
Mochokidae	*Synodontis macropunctata* (n=13)	0.86-0.98	Wright and Page 2008
Batrachoididae	*Opsanus tau* (n=3)	0.9-1.16	TSC 26A, UF 183966, 107712
Lophiidae	*Lophiodes monodi* (n=3)	0.91-1.19	UF 175109, 232948, 11078

Figures

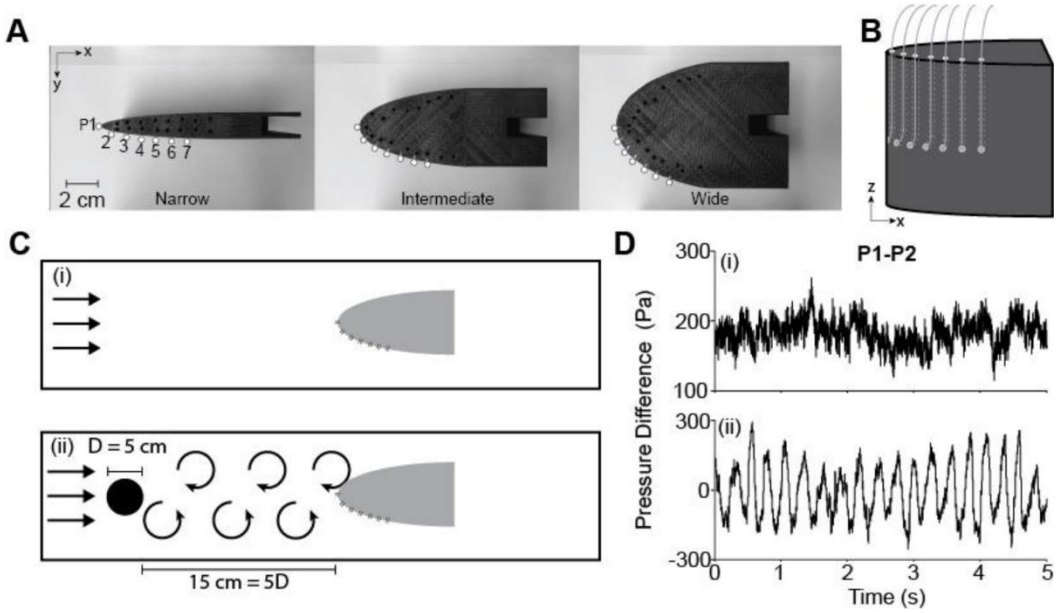

Figure 1. Schematic of model heads, experimental setup, and pressure data collected. (**A**) Dorsal view of the model heads, where white circles indicate positions of the pressure sensors, starting with P1 at the snout. Sensors were spaced 1 cm apart along the head curvature thus sensor position corresponds closely to arc length of head (cm). (**B** Lateral schematic illustrating dorsal insertion sites for sensors, which are then set flush with the lateral surface of the head. (**C**) Schematic of an intermediate-sized model head in steady-state (**i**) and unsteady, vortical (**ii**) flows. (**D**) Example of corresponding pressure difference recordings between sensor P1 and P2 in steady flow (**i**, 52 cm s^{-1}) and in a vortex street (**ii**, where the head was located 5 cm away from a 5 cm diameter cylinder).

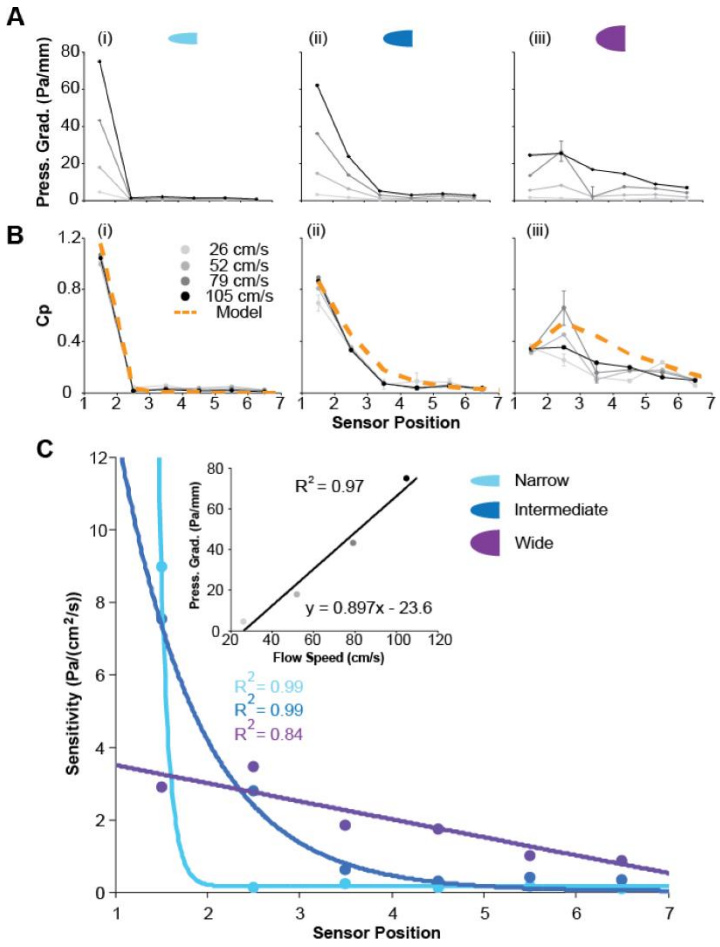

Figure 2. Pressure measurements in steady flow. (**A)** Pressure gradient along the head of (**i**) narrow, (**ii**) intermediate, and (**iii**) wide heads at four flow speeds. (**B**) Measured versus modeled pressure coefficients (C_p vs $\hat{C}_p$) for all heads show a close match for narrow (mean absolute error = 0.04) and intermediate heads (0.06), but not for wide heads (0.12). (**C**) Sensitivity to changes in flow speed decreases posteriorly across sensor position. Values correspond to the slope of a linear fit for pressure gradients across flow speeds (e.g. inset) for the given sensor position. Standard errors were all within 1% of data. All model heads were fit with an exponential curve ($y=ae^{bx}+c$): narrow ($a=1626*10^6$, b=-12.69, c=-0.15), intermediate (a=40.05, b=-1.13, c=0.18), and wide (a=951.8, b=-0.0005, c=-947.8). Light blue, dark blue and purple correspond to narrow, intermediate and wide heads, respectively.

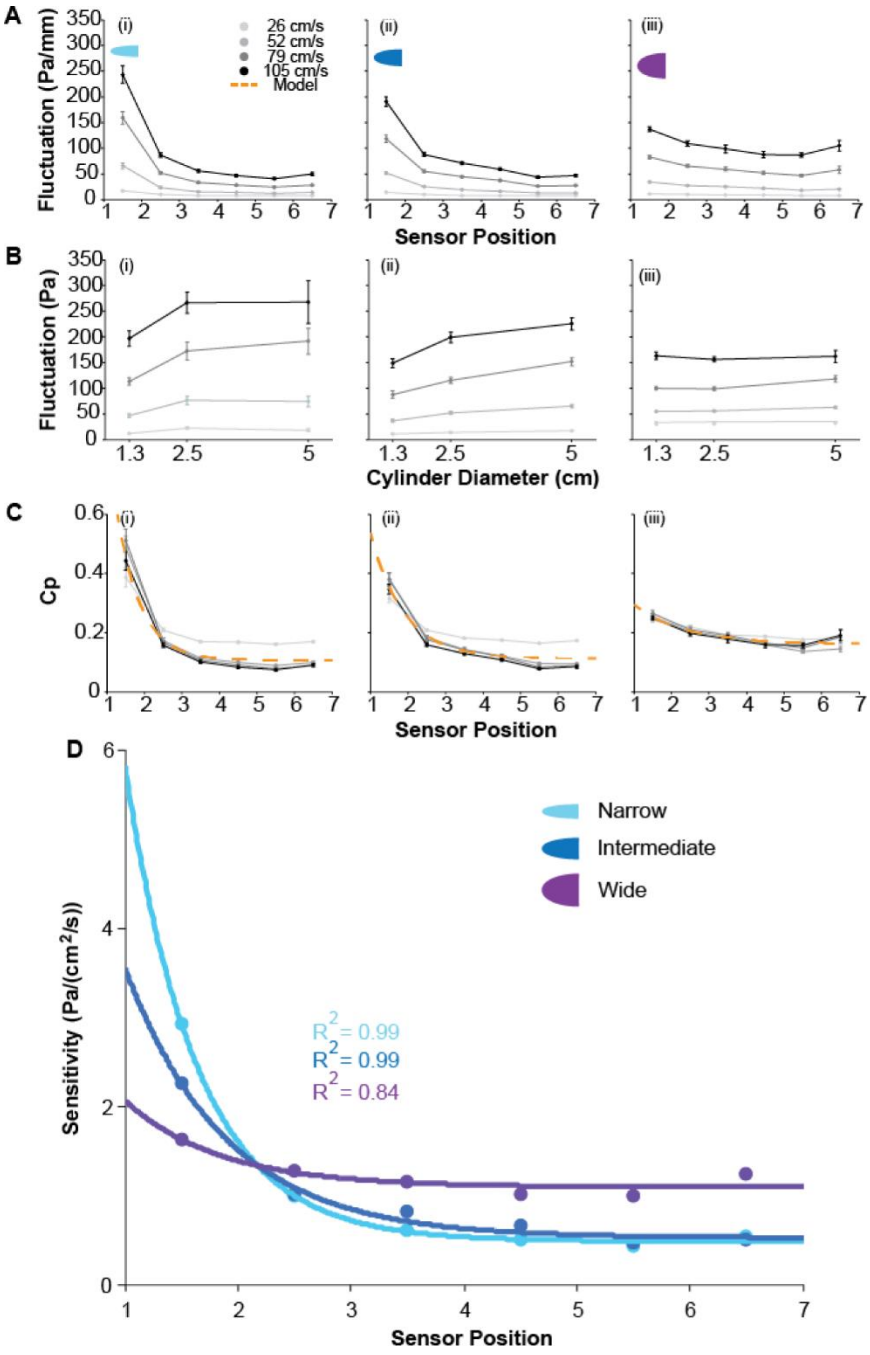

Figure 3. Pressure sensing in a vortex street. (**A**$_{\textbf{i-iii}}$) Pressure fluctuations along narrow, intermediate, and wide heads across four flow speeds. Data points were averaged across all vortex sizes and distances. (**B**) Pressure fluctuations at P1-P2 for (**i**) narrow, (**ii**) intermediate, and (**iii**) wide heads for different cylinder diameters averaged across all distances at four flow speeds. (**Ci-iii**) Measured versus modeled pressure coefficients (C_p vs $\hat{C}_p$) for all heads. Data

points were an average of measurements from all vortex sizes and distances. (**D**) Sensitivity to changes in flow speed decreases posteriorly across sensor position/head arc length. Values correspond to the slope of a linear fit for pressure gradients across flow speeds for the given sensor position. Standard errors were all within 1% of data. All model heads were fit with an exponential curve ($y=ae^{bx}+c$): narrow (a=23.90, b=-1.517, c=0.4672), intermediate (a=9.902, b=-1.175, c=0.5474), and wide (a=3.269, b=-1.198, c=1.089).

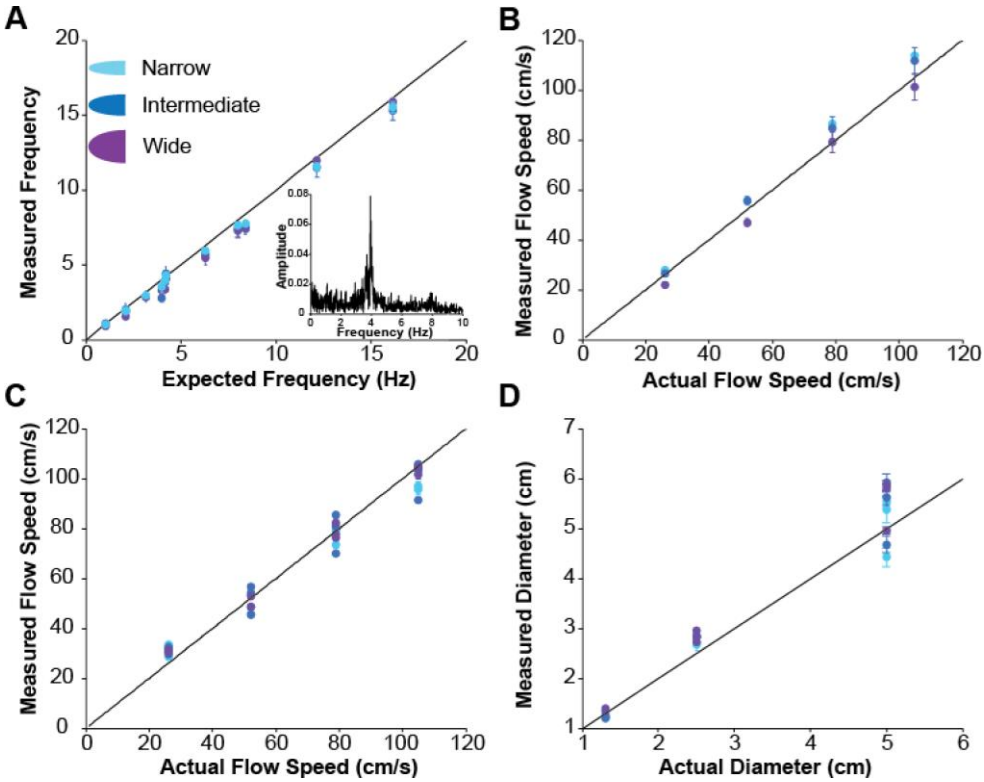

Figure 4. The ability of head sensors to estimate flow parameters and cylinder diameter. (**A**) Measured vortex shedding frequency, determined as the highest amplitude frequency in frequency spectra (e.g. inset figure) for every sensor position, matched the expected vortex shedding frequency. Values represent the average of all vortex shedding frequencies measured across all sensors. (**B**) Steady flow speeds measured by head sensors matched actual flow speeds (determined from a calibrated look up table; Akanyeti and Liao, 2013). All measured values were within 20% error. (**C**) Head sensors could retrieve flow speeds even in vortical flows. For flow speeds >52 cm s^{-1}, values were within 20% error. At the lowest flow speed (26 cm s^{-1}) measured flows were within 30% error. (**D**) Head sensors could estimate the diameter of cylinders that generated vortex streets. All values were within 20% error except for the lowest flow speed (data not shown), which had a higher degree of error.

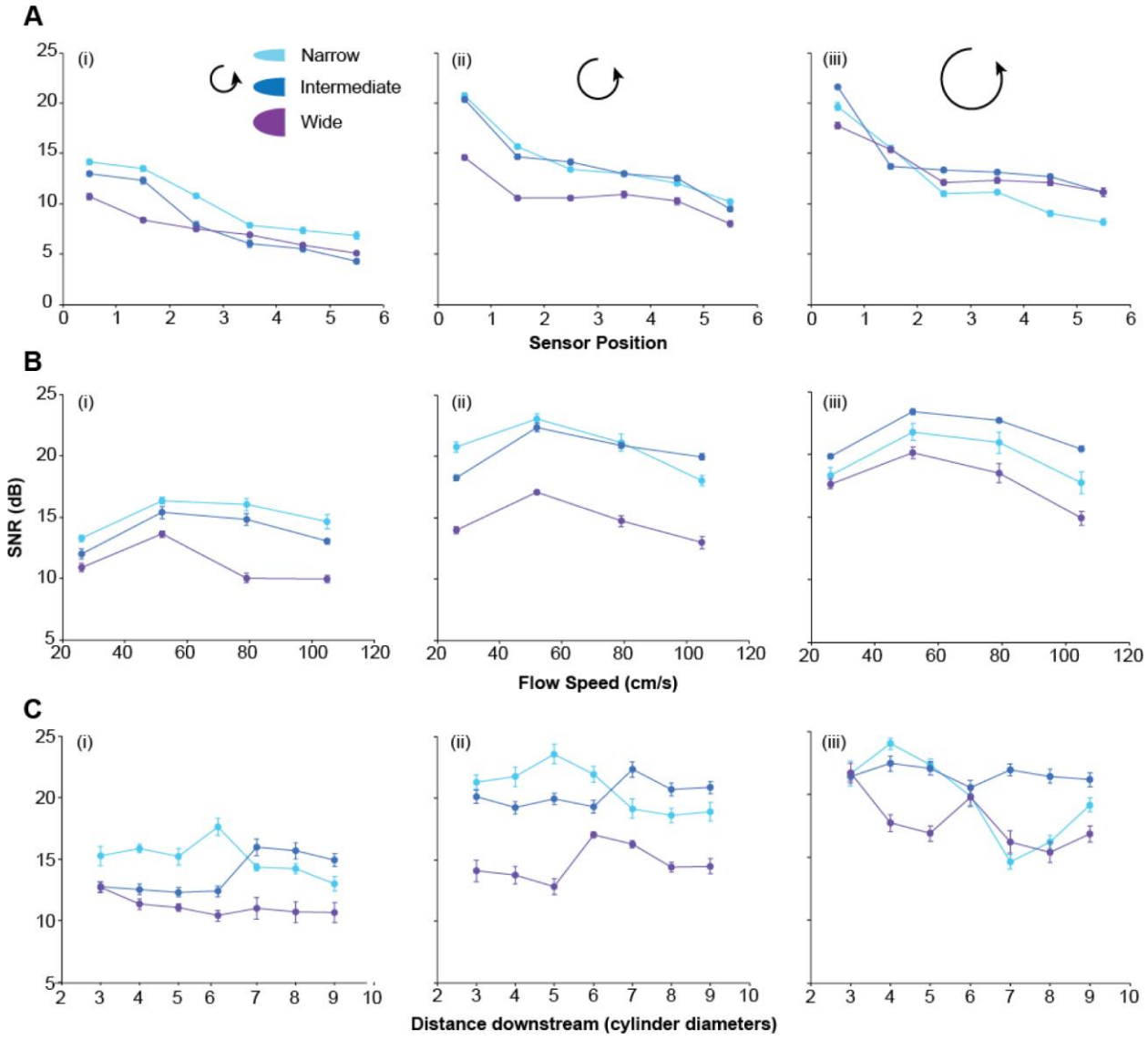

Figure 5. Signal-to-noise ratios (SNR) at different sensor positions, flow speeds, and distance from cylinder. SNR for (**i**) small, (**ii**) medium, and (**iii**) large vortices. (**A**) SNR decreases posteriorly along all model heads (values represent the average of all flow speeds and distances from the cylinder) (**B**) SNR at P1-P2 is generally highest at intermediate flow speeds (values represent the average of all distances (**C**) SNR at P1-P2 is variable depending on the distances of the head from the cylinder. Values were averaged for all flow speeds.

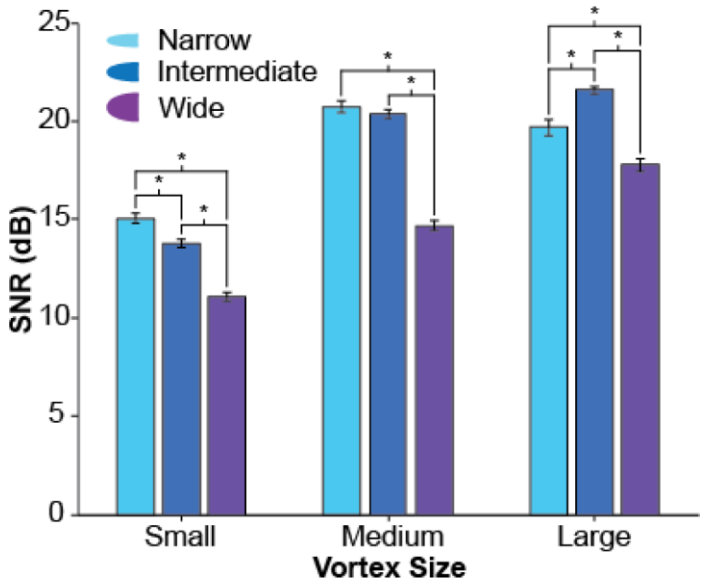

Figure 6. Signal-to-noise ratio determined at P1-P2 for all model head widths. For all vortex sizes tested, narrow and intermediate heads had higher SNRs than wide heads. Narrow heads had the highest SNR for small vortices, while intermediate heads had the highest SNR for large vortices. Values represent averages for all flow speeds and distances. * denotes significance at $p<0.05$ (four-way ANOVA and Tukeys multiple comparison post-hoc test).